CELLULOSE-RICH APRICOT STONE SHELLS AS A SUSTAINABLE BIOSORBENT FOR EFFICIENT CRYSTAL VIOLET DYE REMOVAL: KINETIC AND THERMODYNAMIC INSIGHTS

NAZIHA LADJAL,[*] SMAIL TERCHI,[**] BAHRI DEGHFEL[**] and ABDELHAMID GUELIL[***]

[*]*Higher Normal School of Boussada, Department of Physical Sciences, Boussaada 28201, Algeria*
[**]*Laboratory of Materials and Renewable Energy, Faculty of Sciences, University of Mohamed BOUDIAf - M'Sila, University Pole, Road Bourdj Bou Arreiridj, M'sila 28000, Algeria*
[***]*Department of Chemistry, Faculty of Sciences, University of Biskra, 7000, Algeria*
 Corresponding author: S. Terchi, smail.terchi@univ-msila.dz

Received July 12, 2025

This study explores the potential of apricot stone shells (ASS) as a cost-effective and eco-friendly biosorbent for the removal of Crystal Violet (CV) dye from aqueous solutions. The ASS material was characterized using XRD, FTIR, TG-DTA, and surface area analysis, revealing a composition rich in cellulose, hemicelluloses and lignin, with a high specific surface area of 159 m²/g. Adsorption experiments demonstrated optimal performance at pH≥ 7 and 40 °C, achieving equilibrium within 60 minutes. Kinetic studies indicated a pseudo-second-order mechanism, while the Temkin isotherm best described the adsorption behavior, suggesting chemisorption on heterogeneous sites. Thermodynamic analysis confirmed the endothermic nature of the process, with a Gibbs free energy change (ΔG°) indicating spontaneity at higher temperatures. Remarkably, ASS maintained over 88% adsorption efficiency after four regeneration cycles, highlighting its reusability. These findings position ASS as a promising, sustainable alternative for wastewater treatment, leveraging agricultural waste for effective dye removal.

Keywords: wastewater treatment, apricot stone shells, agricultural waste valorization, Crystal Violet removal

INTRODUCTION

The contamination of water bodies by synthetic dyes is a major environmental issue, particularly in industrial wastewater from textiles, paper, cosmetics, and leather manufacturing. Among these pollutants, Crystal Violet (CV) is one of the most widely used cationic dyes, extensively applied in the dyeing industry, biological staining, and veterinary medicine.[1] However, CV is highly toxic, persistent, and resistant to biodegradation, making its removal from wastewater an urgent challenge.[2] Studies have shown that CV can cause mutagenic and cytotoxic effects on aquatic life and may pose risks to human health due to its carcinogenic potential.[3]

Various physicochemical methods, including chemical oxidation, coagulation, membrane filtration, and advanced oxidation processes, have been employed to remove CV from contaminated water.[4-7] However, these methods often suffer from high costs, energy consumption, and the production of hazardous by-products. Adsorption has been recognized as an efficient and cost-effective technique for removing CV, with activated carbon being the most commonly used adsorbent.[8] However, activated carbon has limitations such as expensive regeneration processes and reduced efficiency after multiple adsorption cycles, making it less sustainable for large-scale applications.[9,10] To address these challenges, researchers have explored low-cost, biodegradable, and renewable biosorbents derived from agricultural waste for CV removal. Several agricultural by-products, such as lime peels,[11] cedar cones,[12] peanut husk[13] and corn cobs,[14] have shown promising adsorption capacities for CV, offering a sustainable alternative to synthetic adsorbents. However, very few studies have explored the potential of apricot stone seeds for dye removal, despite their high availability and promising adsorption properties.

In this study, we introduce the local apricot stone seeds as a novel and highly efficient

biosorbent for CV removal from aqueous solutions. Apricot stones are an abundant agricultural by-product that has been largely underutilized in environmental applications. To the best of our knowledge, this is the first study investigating the potential of apricot stone seeds for CV adsorption, particularly focusing on their reusability and regeneration capacity. Unlike many biosorbents that degrade after a single use, this research explores the desorption and reusability of apricot stone seeds across multiple adsorption cycles, making them a practical and sustainable option for wastewater treatment. The strong contributions of this study include high efficiency CV removal, sustainability and waste valorization and reusability potential.

This study not only addresses the urgent need for cost-effective and sustainable wastewater treatment solutions, but also advances research on agricultural biomass-based adsorbents with potential industrial applications. The findings have significant implications for scaling up green, low-cost adsorption technologies for dye removal, offering an efficient and environmentally friendly solution to CV pollution.

EXPERIMENTAL

Materials

Crystal Violet was supplied by Biochem Chemopharma Company (France). Table 1 summarizes its chemical name, chemical formula, structural formula, maximum absorption wavelength (λ_{max}), molar mass, water solubility, and pH.

Apricot fruits were sourced from a farm located in Metarfa, M'Sila province, Algeria. The stones were first carefully separated from the fruit pulp and thoroughly washed with distilled water to remove any loosely attached residues. To ensure complete removal of organic remnants, dust, and suspended impurities, the cleaned stones were then immersed in a hydrogen peroxide (H_2O_2) solution, which served as an oxidizing agent to assist in surface decontamination.

After the treatment, the stones were rinsed again with water, and the outer shells were manually separated using a mortar and pestle. The isolated stones shells were subsequently dried in an oven at 80 °C for 6 hours to eliminate residual moisture. Once dried, the shells were ground into a fine powder using a mechanical grinder, and sieved to obtain particles with sizes smaller than 80 μm. This fine powdered material was designated as apricot stone shell (ASS) adsorbent, ready for further characterization and adsorption experiments.

Table 1
Physicochemical properties of Crystal Violet

Chemical name	Tris(4-(dimethylamino)phenyl)methylium chloride
Chemical formula	$C_{25}H_{30}N_3Cl$ 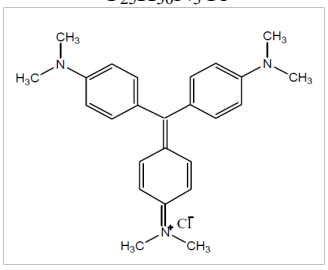
Molar mass ($g \cdot mol^{-1}$)	407.97
Molecular size ($Å^3$)	9.7^3
λ_{max} (nm)	590
Solubility in water at 20 °C ($g \cdot L^{-1}$)	9
pH (5mg·L^{-1}, H_2O, 20°C)	6.8

Characterization methods

Fourier transform infrared spectroscopy (FTIR)

The samples were combined with KBr and compacted under 7 tons into a disc for analysis with a FTIR spectrometer (Shimadzu spectrophotometer (FTIR-8300)). The infrared spectra were recorded between 400 and 4000 cm^{-1} with a resolution of 2 cm^{-1} with 64 scans.

X-ray diffraction (XRD) analysis

X-ray diffraction (XRD) measurements were performed on a Philips PW1710 diffractometer using Cu K_α radiation (λ = 1.54 Å). Data were collected in reflection mode over a 2θ range of 5° to 70°, with 0.02° step increments, 10 s counting time per step, and a sample rotation speed of 0.001° s^{-1}.

TG/DTA analysis

Thermogravimetric (TG) and differential thermal analysis (DTA) were conducted using a DW5470H63 STA analyzer under a nitrogen atmosphere. The samples were heated from room temperature to 800 °C at a controlled rate of 10 °C min^{-1}.

Determination of point of zero charge (pH_{pzc})

To determine the point of zero charge (pH_{pzc}), 0.075 g of the biomass was suspended in 25 mL of 0.01 M NaCl solution. The initial pH of each suspension was adjusted between 2 and 12, after which the samples were agitated at 20 °C for 48 hours. Upon reaching equilibrium, the final pH was recorded and the change in pH ($\Delta pH = pH_{final} - pH_{initial}$) was plotted against the initial pH. The pH_{pzc} corresponds to the initial pH at which ΔpH equals zero.

Determination of specific surface area by Methylene Blue adsorption

In this study, Methylene Blue (MB) was utilized to determine the specific surface area (SSA) of biomass materials. In its aqueous state, MB is a cationic dye ($C_{16}H_{18}N_3S^+$) that readily adsorbs onto negatively charged biomass surfaces. The MB molecule has a rectangular shape with dimensions of 17 Å × 7.6 Å × 3.25 Å, and it is generally assumed to orient itself along its largest surface upon adsorption. The surface area occupied by a single MB molecule is estimated to be approximately 17Å×7.6Å≈ 130 $Å^2$. The MB adsorption experiments were conducted using 50 mg of biomass in 25 mL of MB solutions with initial concentrations ranging from 10 to 300 mg/L. The pH of the suspensions was adjusted to 6 using 1 mol/L nitric acid or sodium hydroxide solutions. Equilibrium adsorption was achieved after 18 hours of stirring at 20 °C and 300 rpm. Following filtration, the equilibrium concentrations of MB were determined spectrophotometrically at 665 nm (Shimadzu UV-2101PC). Using a calibration curve with a high regression coefficient (0.999), the equilibrium MB concentration was calculated as:

$$C_e = (Abs - 0.0029)/0.2 \quad (1)$$

The amount of MB adsorbed (q_e) was determined based on the difference between the initial and equilibrium concentrations, given by:

$$q_e = (C_i - C_e) \times V/m \quad (2)$$

where q_e is the adsorbed MB per unit mass of ASS (mg/g), C_i and C_e are the initial and equilibrium MB concentrations (mg/L), m is the mass of biosorbent used (0.1 g), and V is the solution volume (50 mL).

The adsorption isotherms were modeled using the Langmuir equation in its linearized form:

$$C_e/q_e = 1/(k_L q_m) + C_e/q_m \quad (3)$$

where k_L is the Langmuir constant, and q_m (mg/g) represents the maximum adsorption capacity. The maximum adsorbed MB amount was used to estimate the specific surface area (SSA) of ASS covered by MB molecules using the equation:

$$SSA\ (Å^2/g) = (q_m \times A_m \times 6.02 \times 10^{23})/M_{MB} \quad (4)$$

where the molecular surface area of MB (A_m) is 130 $Å^2$, and its molecular mass (MMB) is 284 g/mol.[15]

Biosorption experiments of Crystal Violet

The biosorption of the cationic dye (CV) on ASS was studied through batch adsorption experiments. The effects of time (adsorption kinetics), solution pH, biosorbent dose, concentration (equilibrium experiments), and temperature (thermodynamic study) were investigated.

The kinetic study was conducted at 20 °C. Several 20 mL CV solutions with initial concentrations of 20, 40, and 60 $mol \cdot L^{-1}$ were prepared. They were mixed with 40 mg of ASS in well-sealed tubes for agitation. The residual dye concentration in each tube was determined after increasing the contact time (between 2.5 min and 360 min).

To determine the equilibrium of the adsorbent-adsorbate system, it is necessary to study the effect of the biosorbent dose. The dependence of CV biosorption on the biosorbent dosage was studied by varying the quantity of ASS in the range of 1–4 $g \cdot L^{-1}$ while keeping all other parameters constant (pH = 6, C_i = 60 $mg \cdot L^{-1}$, t = 18 h, V = 20 mL, and T = 20 °C).

Studies on the effect of pH were conducted by agitating 20 mL of each dye solution at a concentration of 60 $mg \cdot L^{-1}$ with 40 mg of ASS for 18 h over a pH range of 3 to 10. The pH of the solutions was adjusted with an HNO_3 or NaOH solution using a pH meter. The tubes were homogenized by agitation at 20 °C.

Equilibrium and thermodynamic adsorption experiments were carried out in well-sealed tubes, each containing 40 mg of ASS and 20 mL of CV solution with initial concentrations ranging from 20 to 400 $mg \cdot L^{-1}$ for 18 h at different temperatures (20, 30, and 40 °C). After filtration, the equilibrium CV concentrations were determined by spectrophotometry at 590 nm (Shimadzu U-1240). Based on the calibration curve, which has a high regression coefficient (0.994), the equilibrium CV concentrations were calculated using the following equation:

$$C_e = Abs/0.1551 \quad (5)$$

The amount of CV adsorbed (q_e) was also calculated based on the difference between the initial and equilibrium dye concentrations:

$$q_e = (C_i - C_e) \cdot V/m \quad (6)$$

where q_e is the amount of dye adsorbed per unit mass of ASS ($mg \cdot g^{-1}$), C_i and C_e are the initial and equilibrium dye concentrations ($mg \cdot L^{-1}$), m is the mass of biosorbent used, and V is the solution volume (20 mL). The dye removal percentage (adsorption efficiency) was calculated using the following equation:

$$R\ (\%) = [(C_i - C_e)/C_i] \times 100 \quad (7)$$

RESULTS AND DISCUSSION

Characterization results

XRD results

The X-ray diffraction (XRD) pattern of ASS (Fig. 1) reveals distinct peaks corresponding to lignin, cellulose, and hemicelluloses, providing insights into the structural composition of this lignocellulosic material. A peak at 2θ = 16.68°, attributed to the (101) reflection, indicates the presence of lignin. Lignin typically exhibits broad peaks in XRD patterns due to its amorphous nature. A prominent peak at 2θ = 21.82°, corresponding to the (110) reflection, signifies the crystalline regions of cellulose, specifically cellulose type I.[16] This sharp and intense peak suggests a high cellulose content in apricot stones. A peak at 2θ = 34.51°, associated with the (002) reflection, is indicative of hemicelluloses. Similar to lignin, hemicelluloses are generally considered amorphous, but can exhibit specific diffraction features.

FTIR results

The FTIR spectrum of apricot stone shells (Fig. 2) reveals several characteristic bands. A broad band at 3417 cm^{-1} is attributed to the stretching vibrations of O-H bonds, indicating the presence of hydroxyl groups. These may originate from physically adsorbed water or hydroxyl groups present on the material's surface.[17] A band at 2981 cm^{-1} corresponds to the stretching vibrations of C-H groups in alkyl chains, suggesting the presence of aliphatic compounds.

A band at 1743 cm^{-1} is assigned to the stretching vibrations of C=O bonds in carbonyl groups, commonly associated with esters or carboxylic acids found in components such as hemicelluloses or lignin. A band at 1596 cm^{-1} corresponds to the vibrations of C=C bonds in aromatic rings, characteristic of lignin. A band at 1242 cm^{-1} is attributed to C-O bond vibrations, particularly in methoxy (-O-CH_3) groups present in cellulose.[18] A band at 1041 cm^{-1} is associated with the stretching vibrations of C-O bonds, typical of alcohols, esters, or ethers found in cellulose and hemicelluloses.[19]

These interpretations are consistent with the lignocellulosic composition of apricot stone shells, which are rich in cellulose, hemicelluloses, and lignin.

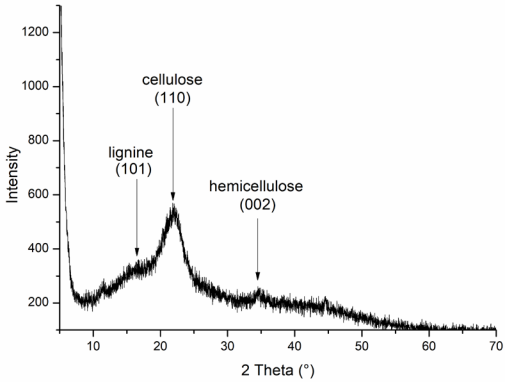

Figure1: XRD pattern of ASS

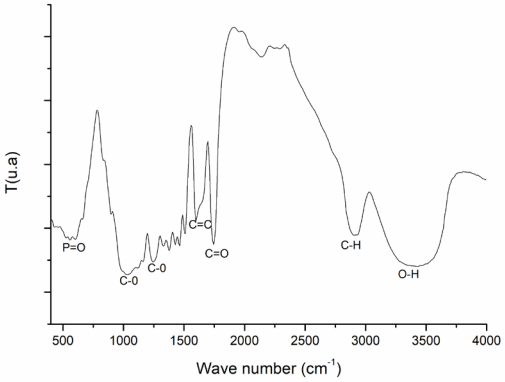

Figure 2: FTIR spectra of ASS

Point of zero charge (pH_{PZC}) determination

The point of zero charge (pH_{pzc}) is an important parameter that represents the pH at which the adsorbent's surface carries no net charge. When the pH is greater than the pH_{pzc}, the surface becomes negatively charged, whereas it is positively charged when the pH is lower than the pH_{pzc}. For the ASS, the pH_{pzc} was determined to be at pH 7 (Fig. 3).

Determination of specific surface area by methylene blue adsorption

The equilibrium adsorption isotherms of MB on ASS for SSA measurement is represented in Figure 4. The specific surface area of the ASS biosorbent was determined to be 159 m^2/g, which is considered relatively high for natural, low-cost materials. A large surface area is crucial in adsorption processes because it directly correlates with the number of available active sites where adsorbate molecules, such as CV dye, can bind. The greater the surface area, the more interactions can occur between the adsorbent and the dye molecules, leading to higher adsorption capacities. Furthermore, the porous nature associated with such a surface area facilitates easier diffusion of dye molecules into the internal structure of the adsorbent. This characteristic not only enhances

the adsorption rate, but also improves the efficiency and effectiveness of the biosorption process. Therefore, the substantial surface area of ASS plays a vital role in its performance as an efficient adsorbent for wastewater treatment applications.

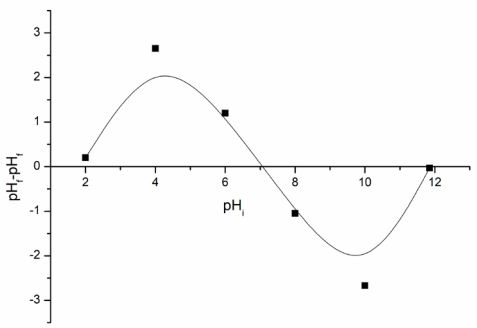

Figure 3: Determination of the isoelectric point (pH_{pzc}) for ASS

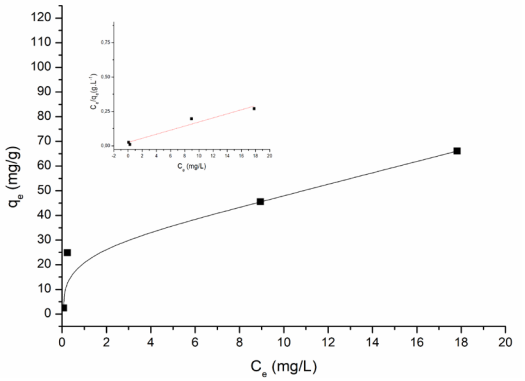

Figure 4: Equilibrium adsorption isotherms of MB on ASS for SSA measurement

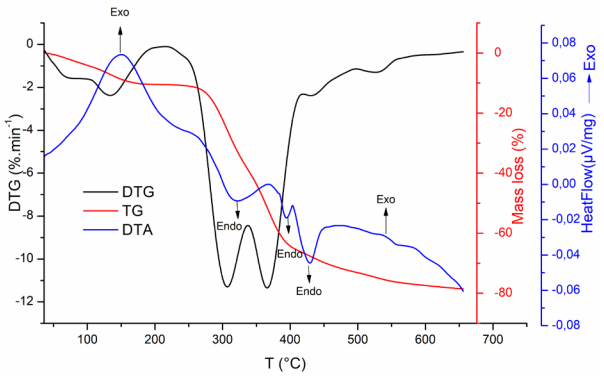

Figure 5: TG, DTG and DTA curves of ASS

TG/DTG results

The thermogravimetric (TG) and derivative thermogravimetric (DTG) analysis of apricot stone shells (Fig. 5) reveals distinct stages of mass loss that reflect the decomposition of specific components within the biomass. The first mass-loss region, extending from ambient temperature to approximately 105 °C with a DTG maximum near 73 °C (~5% mass loss), corresponds to the evaporation of physically adsorbed water present in the apricot stone shells surface. This is followed by a second minor mass-loss stage between 105 °C and 200 °C (DTG peak at ~134 °C), which can be attributed to the release of low molecular weight volatile compounds and bound water. The major pyrolytic decomposition of the biomass occurs between 220 °C and 340 °C, with a maximum rate of mass loss (~18) at around 305 °C, is characteristic of hemicellulose decomposition and amorphous polysaccharide component of the biomass. A more pronounced mass-loss step occurs between 340 °C and 415 °C (DTG peak at ~364 °C with ~28% mass loss), corresponding to the decomposition of cellulose.[17] Above 415 °C, a broader and slower mass-loss region is observed up to approximately 500 °C (DTG maximum at ~435 °C with ~6% mass loss), which is associated with the lignin decomposition over a wide temperature range due to its complex aromatic structure. Finally, the region between 500 °C and 560 °C (maxima at 435 °C with ~4% mass loss) exhibits additional mass loss, likely resulting from the decomposition of residual lignin and the formation of stable char and inorganic ash.[20]

These interpretations align with the typical thermal degradation behavior of lignocellulosic biomass, where hemicellulose decomposes at lower temperatures, followed by cellulose, and then lignin over a broader temperature range.

DTA results

Differential thermal analysis (DTA) of apricot stone shells (Fig. 5) reveals specific thermal events that correspond to the decomposition of various biomass components. The first notable feature is an exothermic peak at ~150 °C, which is likely associated with the oxidation of volatile organic compounds released during the initial heating

phase. Three successive endothermic peaks appear at approximately at ~315 °C, ~394 °C, and ~430 °C: These peaks correspond to the thermal decomposition of hemicelluloses, cellulose, and lignin, respectively. At higher temperatures, an exothermic peak is observed at ~535 °C, which is associated with the oxidation of the residual char formed from previous decomposition stages.

These interpretations align with the typical thermal behavior of lignocellulosic biomass, where moisture evaporation, decomposition of hemicelluloses, cellulose, and lignin, and subsequent oxidation of char residues occur in distinct temperature ranges.

Dye adsorption results

Kinetic study

The influence of contact time (0–360 min) on biosorption capacity of CV was examined at three different initial dye concentrations (20, 40, and 60 mg/L). The experimental results are illustrated in Figure 6. The biosorption capacity increased rapidly within the first 5 minutes, reaching 9.2 mg/g at 20 mg/L, 17.5 mg/g at 40 mg/L, and 24.5 mg/g at 60 mg/L.

Beyond this initial phase, the rate of biosorption slowed but remained continuous for all dye concentrations until equilibrium was achieved at 60 minutes. The rapid initial uptake of dye can be attributed to the high availability of unsaturated active sites, which corresponds to an elevated biosorbent utilization coefficient.[21] The attainment of equilibrium within less 60 minutes indicates that ASS is an efficient biosorbent for CV removal, requiring relatively short contact times to reach maximum adsorption capacity. This efficiency is advantageous for practical wastewater treatment applications, where time and cost are critical factors. Similar equilibrium times have been observed in studies using pineapple leaf powder and apricot seed shell as biosorbents for CV and Acid Blue193, respectively, further supporting the efficacy of agricultural waste materials in dye removal processes.[22,23]

The observed increase in biosorption capacity with higher initial dye concentrations suggests that more CV molecules are available to interact with the active sites on the ASS. This leads to a higher driving force for mass transfer, resulting in increased adsorption.

The pseudo-first order kinetic model, pseudo-second order, Elovich equation and intraparticle diffusion models were used to examine the adsorption kinetics:

The pseudo-first order kinetic model equation:

$$\ln(q_e - q_t) = \ln q_e - k_1 t \quad (8)$$

where q_t and q_e are, respectively, the adsorption amount at instant t and at equilibrium ($mg.g^{-1}$), t is the contacting time (min) and k_1 is the kinetic coefficient (min^{-1}).

The pseudo-second order kinetic model equation:

$$t/q_t = 1/k_2 q_e^2 + t/q_e \quad (9)$$

where k_2 is the kinetic coefficient ($g.mg^{-1}.min^{-1}$).

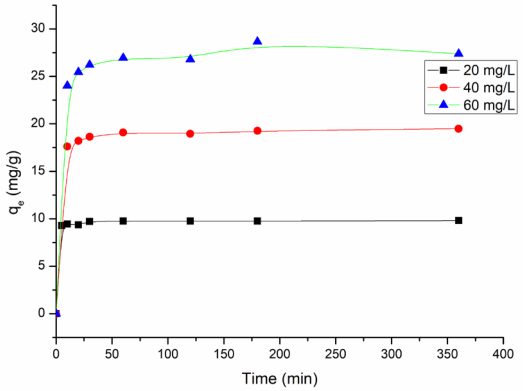

Figure 6: Adsorption kinetics of Crystal Violet on ASS

The Elovich equation is simply written as:

$$q_t = \ln(\alpha\beta) + (1/\beta)\ln t \quad (10)$$

where the α and β, constants of the Elovich model, are attributed to the initial adsorption rate and depict of the extent of surface coverage, respectively.

The intraparticle diffusion model equation:

$$q_t = K_d \cdot t^{0.5} + C \quad (11)$$

where k_d: intraparticle diffusion rate constant ($mg/g \cdot min^{0.5}$), C: intercept, which gives an idea about the boundary layer thickness.

According to the experimental results, these various kinetic models were applied to evaluate the adsorption rate, and the corresponding data are presented in Table 2. Among the models tested, including the pseudo-first order, intraparticle diffusion, and Elovich models, the pseudo-second order kinetic model provided the best fit to the experimental data, as indicated by its highest correlation coefficient (R^2) value, which was very close to 1. In contrast, the other models exhibited significantly lower R^2 values, indicating a weaker correlation with the experimental data.

The pseudo-second order model accurately described the adsorption process over the entire contact time range (0–360 min). Moreover, the theoretical adsorption capacities calculated using this model: 9.90 $mg \cdot g^{-1}$ (C_0 = 20 $mg \cdot L^{-1}$), 19.60 $mg \cdot g^{-1}$ (C_0 = 40 $mg \cdot L^{-1}$), and 27.80 $mg \cdot g^{-1}$ (C_0 = 60 $mg \cdot L^{-1}$) were in close agreement with the experimental values of 9.60, 19.34, and 28.70 $mg \cdot g^{-1}$, respectively. These results confirm that the adsorption kinetics follow a pseudo-second order model. The kinetic model fitting curves are illustrated in Figure 7.

Effect of pH

The effect of pH on the biosorption of CV onto ASS is illustrated in Figure 8, showing a decrease in adsorption capacity under acidic conditions. The reduction can be attributed to the pH-dependent surface charge of the ASS and the ionic nature of the dye. Since CV is a cationic dye, its adsorption is significantly influenced by the surface charge of the adsorbent.

The pH_{pzc} of the ASS is around 7, indicating that at pH < 7, the surface of the adsorbent becomes positively charged due to the protonation of functional groups (such as hydroxyl and carboxyl groups). This results in electrostatic repulsion between the positively charged CV molecules and the adsorbent, leading to lower adsorption capacity.

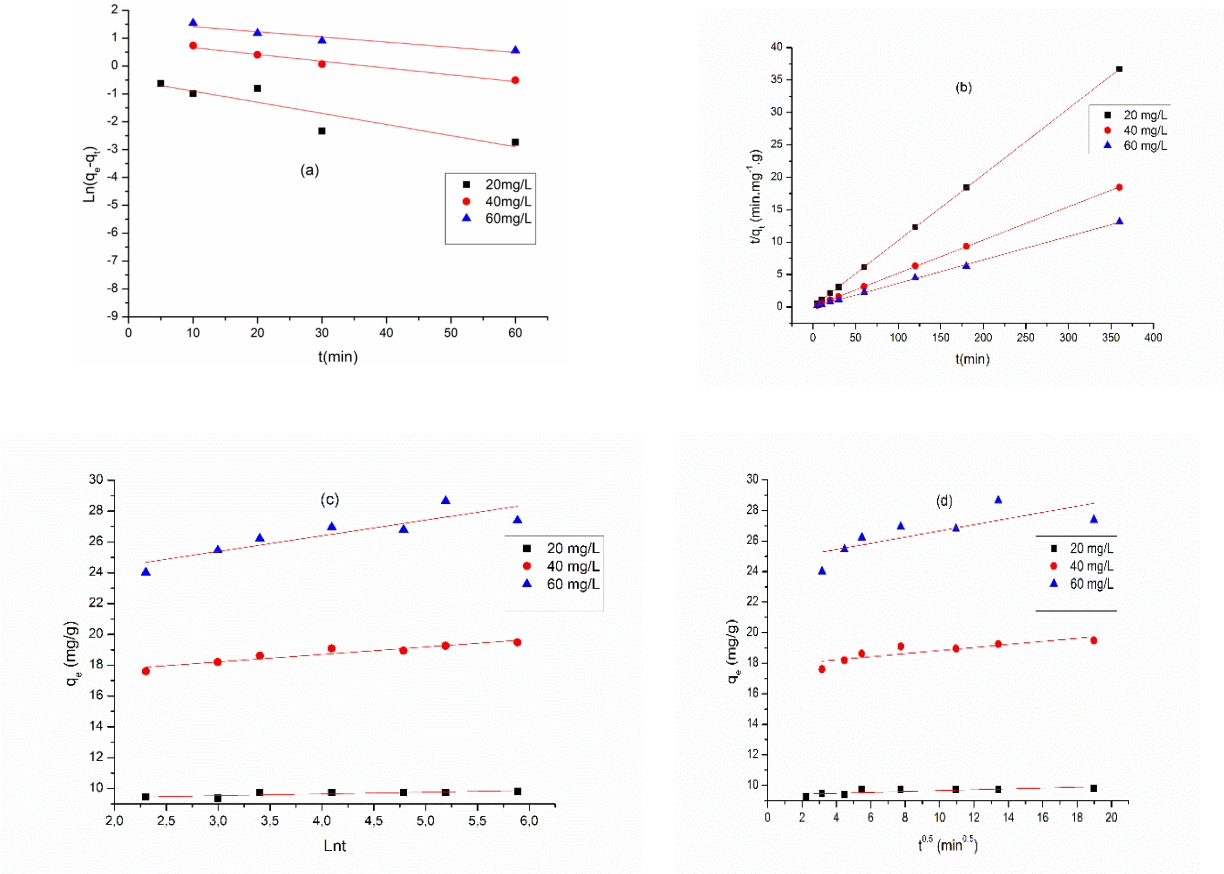

Figure 7: Kinetic modeling of CV adsorption onto ASS: (a) pseudo-first order model, (b) pseudo-second order model, (c) Elovich equation, and (d) intraparticle diffusion model

Table 2
Kinetic constants for CV dye adsorption onto ASS

C_0 (mg/L)	$q_{e,exp}$ (mg/g)	Pseudo-first order model			Pseudo-second order model			Elovich equation			Intraparticle diffusion model	
		$q_{e,the}$	K1	R2	$q_{e,the}$	K_2	R_2	α (mg/g.min)	β	R_2	K_d (mg/g·min0.5)	R_2
20	9.60	1.64	0.034	0.755	9.90	0.176	0.999	0.0011	8.880	0.617	0.028	0.548
40	19.34	2.46	0.024	0.966	19.60	0.0360	0.999	8.252	2.061	0.871	0.100	0.689
60	28.70	4.68	0.018	0.875	27.80	0.0391	0.999	304.878	0.984	0.728	0.201	0.515

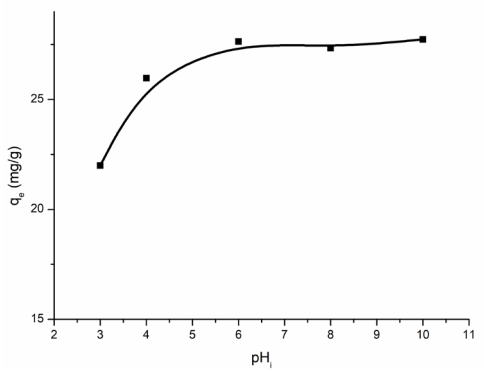

Figure 8: pH-dependent adsorption of Crystal Violet onto ASS

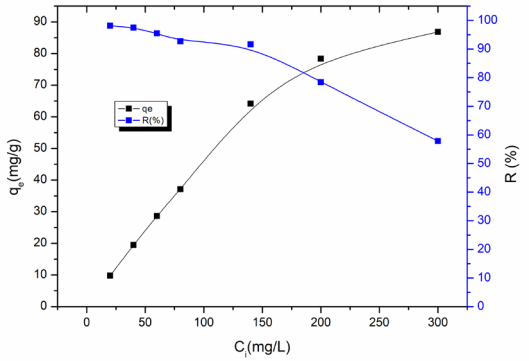

Figure 9: Variation of adsorption capacity and dye removal percentage of CV onto ASS as a function of initial dye concentration at 20 °C

At pH > 7, the surface of the adsorbent acquires a negative charge, enhancing electrostatic attraction between the negatively charged adsorbent and the cationic dye, thereby increasing adsorption. This trend is consistent with previous studies on the biosorption of cationic dyes onto bio-based adsorbents, where adsorption efficiency tends to decrease in acidic environments due to charge repulsion effects.[12,24]

Effect of initial CV dye concentration

The variation of adsorption capacity (q_e) and removal efficiency (R%) of CV dye at equilibrium as a function of the initial dye concentration at 20 °C is presented in Figure 9. As shown, at initial concentrations (≤ 150 mg·L^{-1}), the adsorption efficiency remains high, exceeding 93%. The adsorption capacity (q_e) increases significantly from 10.31 mg·g^{-1} at an initial concentration of 20 mg·L^{-1} to 71.10 mg·g^{-1} at 150 mg·L^{-1}. However, as the initial dye concentration increases beyond 150 mg·L^{-1}, the removal efficiency gradually declines from 93% to 58.13%, while the adsorption capacity continues to rise, reaching 86.39 mg·g^{-1} at 300 mg·L^{-1}. This behavior suggests that the adsorbent sites become progressively saturated at higher concentrations.

Adsorption isotherms

Adsorption isotherms at equilibrium are commonly illustrated by plotting the amount of adsorbate on the solid phase against its concentration in the liquid phase. To describe the interactions between the adsorbent and adsorbate, various theories have been developed, leading to the formulation of different adsorption equilibrium isotherms. This paper examines several single-component adsorption isotherm models, including the Langmuir (L), Freundlich (F), Dubinin–Radushkevich (D–R)[25] and Temkin (T)[23] isotherms.

These isotherms are expressed through the following equations: the Langmuir isotherm, which assumes monolayer adsorption on a surface with a finite number of identical sites, is represented by the equation:

$$\frac{q_e}{q_m} = \frac{k_L C_e}{1+kC_e} \quad (12)$$

In this equation, q_e represents the amount of dye adsorbed per unit mass of adsorbent (mg·g^{-1}), C_e is the equilibrium concentration of dye in the solution (mg·L^{-1}), q_m (mg·g^{-1}) denotes the maximum adsorption capacity corresponding to complete monolayer coverage, and k_L is the Langmuir constant, which is related to the energy or net enthalpy of adsorption.

The Freundlich isotherm, which is applicable to adsorption on heterogeneous surfaces, is expressed by the following equation:

$$q_e = k_f C_e^{\frac{1}{n}} \quad (13)$$

In this model, K_f and n are the Freundlich constants, where K_f relates to the adsorption capacity and n indicates the adsorption intensity.

The Temkin isotherm model is defined by the following relationship:

$$q_e = \frac{RT}{b} \mathrm{Ln}(K_T C_e) \quad (14)$$

This model assumes that the heat of adsorption decreases linearly with increasing surface coverage due to adsorbent–adsorbate interactions. It is characterized by two constants: K_T, the Temkin equilibrium binding constant (L·g^{-1}), and b is a constant related to the variation in adsorption energy (J·mol^{-1}).

The Dubinin–Radushkevich (D–R) isotherm model does not assume a homogeneous surface or a constant sorption potential, unlike other isotherm models. Notably, the D–R model is considered more general than the Langmuir isotherm in describing adsorption behavior. The D–R isotherm is represented by the following equations:

$$q_e = q_m e^{-(B\varepsilon^2)} \quad (15)$$

$$\varepsilon = RT\ln\left(1+\frac{1}{C_e}\right) \quad (16)$$

where B is a constant related to the adsorption energy (mol^2·J^{-2}), q_m represents the theoretical adsorption capacity (mg·g^{-1}), and ε is the Polanyi potential.

The experimental adsorption isotherms of CV dye at various temperatures (20, 30, and 40 °C) are presented in Figure 10 (a). To analyze the equilibrium behavior, the experimental data were fitted to four nonlinear isotherm models: Langmuir (Eq. 12), Freundlich (Eq. 13), Temkin (Eq. 14), and Dubinin–Radushkevich (D–R) (Eq. 15) and plotted (Fig. 10 (b-d)). The estimated model parameters, along with their corresponding coefficients of determination (R^2), are summarized in Table 3. It is important to note

that the model parameters were obtained through an iterative nonlinear regression approach. As a result, the generation of graphical plots for these fittings was deemed unnecessary and thus not provided.

The performance and validity of each isotherm model were assessed primarily based on the R^2 values. Among the tested models, the Temkin isotherm exhibited the highest R^2 across all studied temperatures, indicating the best fit to the experimental data. This finding suggests that the adsorption process involves a monolayer distribution of CV dye molecules onto the ASS surface, occurring on energetically heterogeneous sites. Furthermore, the Temkin model implies that the binding energy between the biosorbent and the solute remains relatively uniform, highlighting consistent interactions throughout the adsorption process.[26]

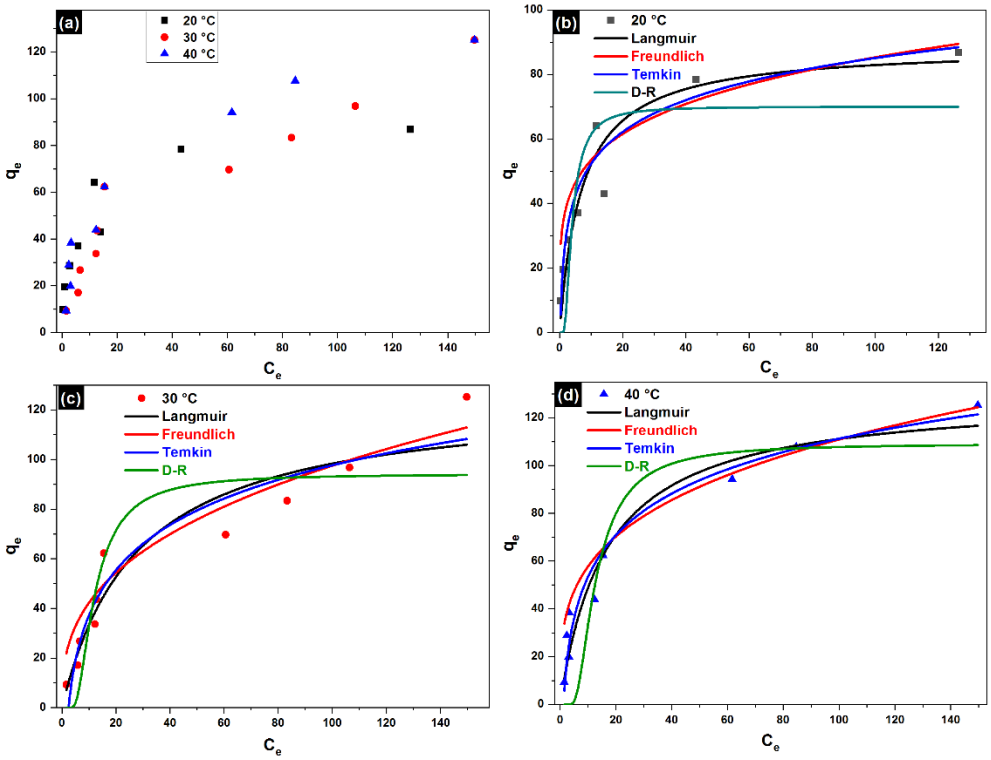

Figure 10: Experimental adsorption isotherms of CV dye onto ASS at different temperatures (a), with corresponding model fits (full lines) for Langmuir, Freundlich, Dubinin–Radushkevich (D–R), and Temkin isotherms at 20 °C (b), 30 °C (c), and 40 °C (d)

Table 3
Isotherm model parameters

Model	20 °C	30 °C	40 °C
Langmuir: $\frac{q_e}{q_m} = \frac{k_L C_e}{1+kC_e}$	$q_m = 88.73253$ $k_L = 0.14256$ $R^2 = 91.34\%$	$q_m = 125.53796$ $k_L = 0.03617$ $R^2 = 90.95\%$	$q_m = 129.5272$ $k_L = 0.06043$ $R^2 = 94.74\%$
Freundlich: $q_e = k_f C_e^{\frac{1}{n}}$	$k_f = 33.51751$ $n = 4.92858$ $R^2 = 88.23\%$	$k_f = 18.30757$ $n = 2.75289$ $R^2 = 95.73.23\%$	$k_f = 30.02662$ $n = 2.75289$ $R^2 = 93.10\%$
Temkin: $q_e = \frac{RT}{b} Ln(K_T C_e)$	K_T=3.95787 b=171.29755 $R^2 = 95.26\%$	K_T=0.41188 b=95.9272 $R^2 = 99.23\%$	K_T=0.837 b=103.60889 $R^2 = 98.52\%$
D-R: $q_e = q_m e^{-(B\varepsilon^2)}$ $\varepsilon = RTln\left(1+\frac{1}{C_e}\right)$	$q_m = 70.05277$ $B = 2.43984.10^{-6}$ $R^2 = 70.27\%$	$q_m = 94.2334$ $B = 1.83437.10^{-5}$ $R^2 = 82.14\%$	$q_m = 109.1611$ $B = 1.93963.10^{-5}$ $R^2 = 86.24\%$

The results clearly show that increasing the temperature from 20 °C to 40 °C leads to a noticeable enhancement in the adsorption capacity, indicating that 40 °C represents the optimum temperature for the adsorption process.

Thermodynamic study

The thermodynamic parameters, including changes in Gibbs free energy (ΔG°), enthalpy (ΔH°), and entropy (ΔS°), at three different temperatures were used to describe the thermodynamic behavior of CV dye adsorption onto ASS. To calculate these parameters and determine the Gibbs free energy at the three temperatures, the Gibbs equation was used:

$$\Delta G° = -RT\ln K_d \quad (17)$$

where R is the constant of perfect gas (8.314 $J \cdot mol^{-1} \cdot K^{-1}$), T is the absolute temperature of the adsorbent–adsorbate suspension (K), K_d is the distribution coefficient, expressed as $K_d = q_e/C_e$, calculated at a given surface coverage rate $\theta = q_e/q_m$. Here, q_e and q_m represent the equilibrium adsorption capacity and the maximum monolayer adsorption capacity ($mg \cdot g^{-1}$), respectively, and C_e is the equilibrium concentration of the dye in solution ($mg \cdot L^{-1}$). The value of K_d was calculated at $\theta = 0.9$ for the three isotherms.

The relationship between ΔG°, ΔH° and ΔS° is given by:

$$\Delta G = \Delta H - T\Delta S \quad (18)$$

Substituting Equation 17 into Equation 18, the well-known van't Hoff equation was obtained:

$$\ln K_d = -\Delta H°/RT + \Delta S°/R \quad (19)$$

The enthalpy (ΔH°) and entropy (ΔS°) changes associated with the adsorption process were determined from the slope and intercept of the linear plot of $\ln K_d$ versus 1/T, where the slope corresponds to -ΔH°/R and the intercept to ΔS°/R. The plot of $\ln K_d$ as a function of 1/T, along with the calculated thermodynamic parameters, is presented in Figure 11 and Table 4, respectively. The positive ΔH° value of 23.10 $kJ \cdot mol^{-1}$ confirms that the adsorption of the CV dye is endothermic. Additionally, the positive ΔS° value of 75.45 $J \cdot mol^{-1} \cdot K^{-1}$ indicates an increase in disorder at the solid-liquid interface during the adsorption process. The decreasing values of ΔG° with rising temperature indicate that the adsorption process becomes more thermodynamically favorable at higher temperatures.

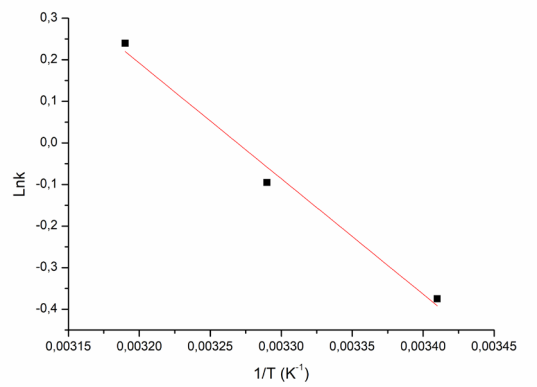

Figure 11: Plot of $\ln K_d$ versus 1/T used for the determination of thermodynamic parameters

Table 4
Thermodynamic constants for the adsorption of CV dye onto ASS at different temperatures

T (K)	ΔG° ($kJ \cdot mol^{-1}$)	ΔH° ($kJ \cdot mol^{-1}$)	ΔS° ($J \cdot mol^{-1} \cdot K^{-1}$)
293.15	0.92		
303.15	0.24	23.10	75.45
313.15	-0.61		

Additionally, the value of ΔH° can provide insight into the nature of the adsorption process: values in the range of 5–50 $kJ \cdot mol^{-1}$ typically indicate physisorption, while those between 50–80 $kJ \cdot mol^{-1}$ suggest chemisorption.[27] Thus, the adsorption of CV dye onto the ASS sample occurs primarily through physical adsorption, driven by van der Waals forces between the nanocomposite and dye molecules. This type of

interaction also results in a relatively high adsorption rate. Consequently, increasing the temperature can enhance the adsorption efficiency of the studied onto the ASS.

Comparison with other adsorbents

Various agricultural biosorbents used for the removal of CV dye have been reviewed and summarized in Table 5 to facilitate a comprehensive comparison with ASS, the novel biosorbent developed in the present study. These biosorbents, derived from diverse agricultural by-products, have shown varying degrees of effectiveness depending on their physicochemical properties and surface characteristics. However, the ASS material demonstrated significantly higher adsorption capacities compared to those previously reported, highlighting its superior affinity for CV dye molecules. This enhanced performance can be attributed to its optimized surface area, functional groups, and pore structure, which collectively contribute to improved dye uptake. The findings of this study clearly establish the potential of ASS as an efficient, low-cost, and sustainable biosorbent capable of removing substantial amounts of CV dye from aqueous solutions. Consequently, ASS emerges as a highly promising candidate for practical applications in the treatment of industrial wastewater, particularly in scenarios involving high levels of dye contamination.

Table 5
Adsorption capacity of various agricultural biosorbents towards CV dye

Adsorbent	Q_m (mg.g^{-1})	Reference
Cedar cone forest waste	8	[12]
Date palm leaves	37.5	[24]
Almond shell	12.2	[28]
Jackfruit leaf powder	43.39	[29]
Pineapple leaves	13.2	[11]
Lime peels	12.8	[11]
Peanut husk	20.95	[13]
Trifolium repens	1.95	[30]
Ausambi peel	9.5	[31]
Coriandrum sativum seeds	1.80	[32]
Apricot stone shells	87.20	This study

Adsorbent reusability

In large-scale water treatment operations, the selection of an adsorbent that is both cost-effective and reusable is paramount to ensure operational sustainability and reduce long-term expenses. Beyond economic considerations, the environmental implications of disposing spent adsorbents are significant, as they may release previously captured contaminants back into the ecosystem, leading to secondary pollution. Therefore, a critical criterion in evaluating suitable adsorbents for wastewater treatment is their regeneration potential and durability over multiple usage cycles.

In this context, the adsorption–desorption performance of ASS material pre-loaded with CV dye was examined. Following the initial adsorption, the saturated adsorbent underwent regeneration through a single rinse with a 50% v/v solution of distilled water and ethanol. Subsequently, the regenerated material was dried at 50 °C for 12 hours. This regenerated ASS adsorbent was then subjected to four consecutive adsorption cycles to assess its reusability. Remarkably, the material maintained a high adsorption efficiency throughout these cycles, with an efficiency of approximately 90% after the fourth cycle, as illustrated in Figure 12. Even in the final cycle, the adsorption capacity remained above 88%, underscoring the material's stability and strong potential for repeated application.

These findings highlight the reusability of ASS as a significant advantage, positioning it as a promising candidate for sustainable wastewater treatment processes. The regeneration and reuse of adsorbents like ASS not only contribute to cost savings, but also align with environmental sustainability goals by minimizing waste generation. Such practices are essential in advancing eco-friendly and economically viable water treatment solutions.

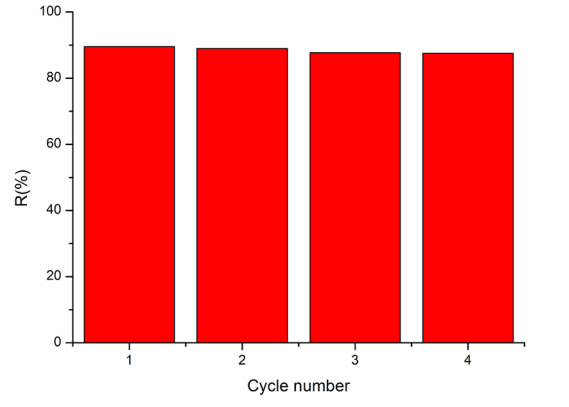

Figure 12: Reusability performance of ASS for the adsorptive removal of CV dye
(C_0: 40 mg L^{-1}; T: 20 °C; t = 1 h, dose of adsorbent:2 g/L)

CONCLUSION

This study successfully demonstrated the potential of ASS as an effective, low-cost biosorbent for the removal of CV dye from aqueous solutions. Comprehensive material characterization confirmed that the ASS is rich in cellulose, hemicelluloses, and lignin, with a notably high specific surface area favorable for adsorption applications. Experimental results highlighted the significant influence of operating parameters: equilibrium was reached within 60 minutes, the biosorption capacity increased at pH ≥ 7, and the adsorption performance improved with temperature, with an optimum at 40 °C. Kinetic modeling indicated a pseudo-second order mechanism, while equilibrium data best fit the Temkin isotherm model, suggesting chemisorption with favorable energetics. Thermodynamic analysis confirmed the endothermic nature of the process. Additionally, the material exhibited good reusability over multiple cycles, underscoring its practical applicability for wastewater treatment. Overall, the ASS emerges as a sustainable and efficient alternative for dye removal, contributing to the valorization of agricultural waste and the advancement of eco-friendly water purification technologies.

ACKNOWLEDGEMENTS: Authors thank the Algerian Ministry of Higher Education and Scientific Research represented by the Thematic Research Agency in Health and Life Sciences (TRAHLS) for financial support under the National Research Programs (NRP).

REFERENCES

[1] M. M. Lazar, R. P. Damaschin, I. Volf and M. V. Dinu, *J. Polym. Environ.*, (2024), https://doi.org/10.1007/s10924-024-03071-3
[2] A. S. A. Wasidi, H. H. E. Feky, R. K. Shah, F. A. Saad and E. A. Abdelrahman, *Sci. Rep.*, **14**, 1 (2024), https://doi.org/10.1038/s41598-024-71981-4
[3] Y. A. Hasanien, A. G. Zaki and A. S. Abdel, *Biomass Convers. Biorefin.*, **15**, 3235 (2025), https://doi.org/10.1007/s13399-023-04991-3
[4] H. A. Haq, T. Javed, M. A. Abid, S. Zafar and M. I. Din, *Desalin. Water Treat.*, **224**, 395 (2021), https://doi.org/10.5004/dwt.2021.27178
[5] Y. Wang, Q. Geng, J. Yang, Y. Liu and C. Liu, *ACS Omega*, **5**, 31137 (2020), https://doi.org/10.1021/acsomega.0c04285
[6] E. S. Mansor, H. Abdallah and A. M. Shaban, *J. Environ. Chem. Eng.*, **8**, 103706 (2020), https://doi.org/10.1016/j.jece.2020.103706
[7] E. V. Vidya Vijay, M. Jerold, M. S. Ramya Sankar, S. Lakshmanan and V. Sivasubramanian, *Water Sci. Technol.*, **79**, 597 (2019), https://doi.org/10.2166/wst.2019.066
[8] J. X. Zhang and L. L. Ou, *Water Sci. Technol.*, **67**, 737 (2013), https://doi.org/10.2166/wst.2012.605
[9] G. Kumar, S. Sen and K. G. Bhattacharyya, *J. Environ. Manage.*, **171**, 1 (2016), https://doi.org/10.1016/j.jenvman.2016.01.038
[10] S. Bentahar, A. Dbik, M. E. Khomri and N. E. Messaoudi, *J. Environ. Chem. Eng.*, **5**, 5921 (2017), https://doi.org/10.1016/j.jece.2017.11.003
[11] R. A. Kristanti, A. Yuniarto and T. Hadibarata, *Int. J. Integr. Eng.*, **14**, 269 (2022), https://doi.org/10.30880/ijie.2022.14.01.025
[12] M. Zamouche, A. Habib, K. Saaidia and M. Bencheikh Lehocine, *SN Appl. Sci.*, **2**, 1 (2020), https://doi.org/10.1007/s42452-020-1976-0
[13] S. Abbas, T. Javeed, S. Zafar, M. B. Taj, A. R. Ashraf *et al.*, *Desalin. Water Treat.*, **233**, 387 (2021), https://doi.org/10.5004/dwt.2021.27538

[14] Y. Song, R. Peng, S. Chen and Y. Xiong, *Desalin. Water Treat.*, **154**, 376 (2019), https://doi.org/10.5004/dwt.2019.24067
[15] S. Terchi, N. Ladjal, B. Zidelkheir and K. Bachari, *Rev. Roum. Chim.*, **65**, 869 (2020), https://doi.org/10.33224/rrch.2020.65.10.02
[16] D. Mohan, A. Sarswat, V. K. Singh, M. Alexandre-Franco and C. U. Pittman, *Chem. Eng. J.*, **172**, 1111 (2011), https://doi.org/10.1016/j.cej.2011.06.054
[17] K. A. Abboudi, *J. Indian Acad. Wood Sci.*, (2017), https://doi.org/10.1007/s13196-017-0197-7
[18] D. Allouch, M. Popa, V. I. Popa, G. Lisa, C. Puițel *et al.*, *Cellulose Chem. Technol.*, **53**, 851 (2019), https://doi.org/10.35812/CelluloseChemTechnol.2019.53.82
[19] R. Han, L. Zhang, C. Song, M. Zhang, H. Zhu *et al.*, *Carbohyd. Polym.*, **79**, 1140 (2010), https://doi.org/10.1016/j.carbpol.2009.10.054
[20] A. Gagliano, F. Nocera, F. Patania, M. Bruno and S. Scirè, *Int. J. Heat Technol.*, **34**, 553 (2016), https://doi.org/10.18280/ijht.34S250
[21] J. Febrianto, A. Natasia, J. Sunarso, Y. Ju, N. Indraswati *et al.*, *J. Hazard. Mater.*, **162**, 616 (2009), https://doi.org/10.1016/j.jhazmat.2008.06.042
[22] S. Chakraborty, S. Chowdhury and P. D. Saha, *Appl. Water Sci.*, **2**, 135 (2012), https://doi.org/10.1007/s13201-012-0030-9
[23] A. Hashem, C. O. Aniagor, O. M. Morsy, A. Abou-Okeil and A. A. Aly, *Biomass Convers. Biorefin.*, **14**, 12283 (2024), https://doi.org/10.1007/s13399-022-03272-9
[24] A. Ghazali, M. Shirani, A. Semnani, V. Zare-Shahabadi and M. Nekoeinia, *J. Mol. Liq.*, **272**, 403 (2018), https://doi.org/10.1016/j.jece.2018.05.043
[25] M. A. da Silva, D. D. S. Dias, J. M. V. Capela, I. A. P. Fertonani and C. A. Ribeiro, *J. Therm. Anal. Calorim.*, **148**, 12321 (2023), https://doi.org/10.1007/s10973-023-12461-1
[26] A. Hashem, *Cellulose*, **28**, 3599 (2021), https://doi.org/10.1007/s10570-021-03726-9
[27] S. H. Tabrizi, B. Tanhaei, A. Ayati and S. Ranjbari, *Environ. Res.*, **204**, 111965 (2022), https://doi.org/10.1016/j.envres.2021.111965
[28] I. Loulidi, F. Boukhlifi, M. Ouchabi, A. Amar, M. Jabri *et al.*, *J. Chem.*, **2020**, 1 (2020), https://doi.org/10.1155/2020/5873521
[29] P. D. Saha, S. Chakraborty and S. Chowdhury, *Colloids Surf. B Biointerfaces*, **92**, 262 (2012), https://doi.org/10.1016/j.colsurfb.2011.11.057
[30] S. Gul, S. Afsar, H. Gul and B. Ali, *J. Iran. Chem. Soc.*, **20**, 2781 (2023), https://doi.org/10.1007/s13738-023-02875-x
[31] S. Jha, R. Gaur, S. Shahabuddin, I. Tyagi and J. Giri, *Clean. Eng. Technol.*, **26**, 100951 (2025), https://doi.org/10.1016/j.clet.2025.100951
[32] M. Naveed, T. Javed and M. Babar, *Desalin. Water Treat.*, **267**, 186–200 (2022), https://doi.org/10.5004/dwt.2022.28628